A Coherent Doppler Profiler for High-Resolution Particle Velocimetry in the Ocean: Laboratory Measurements of Turbulence and Particle Flux

LEN ZEDEL

Physics Department, Memorial University of Newfoundland, St. John's, Newfoundland, Canada

ALEX E. HAY

Oceanography Department, Dalhousie University, Halifax, Nova Scotia, Canada

ABSTRACT

A pulse-to-pulse coherent acoustic Doppler profiler has been developed for high-resolution particle velocimetry in the ocean, in particular for remote measurements of suspended sediment flux and turbulence in the nearshore and continental shelf bottom boundary layer. Acoustic backscatter estimates of suspended particle concentration and velocity are determined simultaneously from the phase and amplitude of the backscattered signal over an $O(1 \text{ m})$-long profile with subcentimeter resolution, at an ensemble-averaged rate of $O(25 \text{ Hz})$. To characterize the performance of the profiler as a remote turbulent flux sensor, laboratory experiments were carried out in a particle-laden high–Reynolds number round jet. The results include comparisons between the acoustic Doppler and standard laboratory sensors, and to previous experimental and theoretical results for turbulent jets. The observed mean radial particle flux profile is found to be consistent with the computed mean flux profile for a turbulent jet. The measured entrainment rate is within 10% of the accepted value for turbulent round jets. Energy spectra of the turbulent motions demonstrate the $-5/3$ slope characteristic of the inertial subrange. The kinetic energy spectral densities obtained with the Doppler profiler match observations with a Sontek acoustic Doppler velocimeter and are in qualitative agreement with hotfilm measurements within the jet. Space–time domain images of particle flux exhibit well-defined coherent structures. Cospectral analysis demonstrates that these larger structures dominate the particle flux.

1. Introduction

The fluxes of sediment, momentum, heat, nutrients, and other quantities at the seabed are of wide importance, touching upon a broad range of fundamental and practical questions in oceanography and in ocean engineering. These fluxes are determined largely by turbulence in the bottom boundary layer. In the nearshore zone and on the continental shelf, it is often the case that bottom boundary layer turbulence is generated by both surface gravity waves and lower-frequency motions, such as tidal and wind-driven currents. A necessary consequence of the flux of momentum from the fluid to the bed is that the surface gravity waves and low-frequency motions are coupled to each other through the bed shear stress. This fact has been known for some time, and various theories for combined-flow boundary layers have been put forward (e.g., Lundgren

1972; Smith 1977; Grant and Madsen 1979; Christoffersen and Jonsson 1985). However, field verification of these theories has remained elusive (e.g., Grant and Madsen 1986; Trowbridge and Agrawal 1995), at least partly because the wave boundary layer is only a few centimeters thick: it has been difficult to obtain vertical profiles of horizontal velocity and turbulence without significant disturbance of the near-bed flow using standard instrumentation. Over mobile sediment beds, the measurement problem is further complicated by significant variations in local bed elevation with time (e.g., Hay and Bowen 1993). Such variations represent the dynamic adjustment of the bed to the fluid forcing and thus are fundamentally part of the phenomenon of interest.

In such environments, acoustic profiling provides an attractive measurement alternative. Depending upon water depth, the sensor can be mounted 1 m or more above bottom, so that the wave boundary layer can be probed remotely. Furthermore, the bed echo is imbedded in the backscatter profile data stream, so that variations in bed elevation are part of the measurement, and the suspended particle measurements are automatically bed referenced. An example of such an application is acoustic

Corresponding author address: Dr. Len Zedel, Physics Department, Memorial University of Newfoundland, St. John's, NF A1B 3X7, Canada.
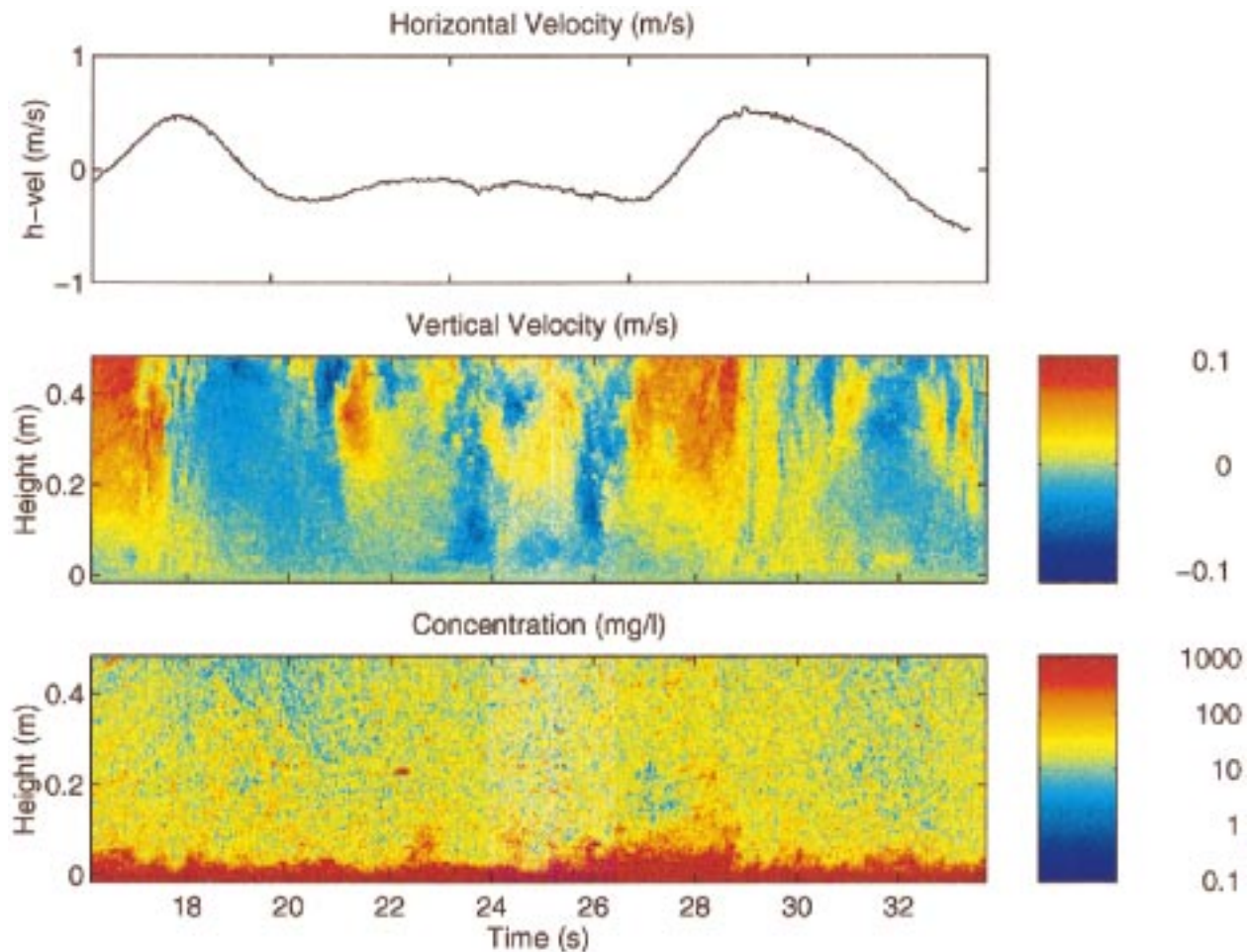E-mail: zedel@claymore.physics.mun.ca

FIG. 1. Example of data collected with the new coherent Doppler profiler in 3-m-deep water 60 m offshore in the bottom boundary layer. (a) the horizontal component of velocity (determined by using measurements from an obliquely directed coherent sonar beam); (b) vertical velocity; (c) concentration.

studies of suspended sediment concentration and size (see, e.g., Lynch and Agrawal 1991; Thorne et al. 1991; Hay and Sheng 1992).

Acoustic systems can also be used to measure velocity structure through the use of Doppler techniques (Pinkel 1980). Typical Doppler sonar systems cannot, however, provide the resolution needed to investigate the details of combined wave–current bottom boundary layers: this requires centimeter-scale vertical resolution, or better. We have developed a new acoustic profiler that provides the enhanced velocity and spatial resolution needed for combined-flow boundary layer studies. The system combines coherent phase measurements with calibrated backscatter amplitude to allow the measurement of suspended sediment concentration and particle velocity profiles with subcentimeter vertical resolution. The concentration and velocity measurements are coincident in space and time and can therefore be combined to provide profiles of instantaneous particle flux. An example of the velocity and suspended sediment structure in the

bottom boundary layer that are revealed with this sensor is shown in Fig. 1. These data were collected during a nearshore sediment dynamics experiment in 3-m water depth at Queensland Beach, Nova Scotia, Canada, during the fall of 1995.

Prior to the Queensland Beach experiment, a series of towtank experiments had been carried out to calibrate and test the operating characteristics of the sensor, and to compare test results with theoretical calculations of expected performance. The results are presented in Zedel et al. (1996). Of particular interest to us were the different contributions to the decorrelation of the signal. Significantly, it was concluded that turbulent velocities should be measurable at scales of oceanographic interest. Indeed, the vertical velocities in Fig. 1 (middle panel) exhibit a wealth of small-scale structures, suggestive of turbulence.

Remote measurements of turbulence and small-scale velocity shear require verification. For this purpose, we have chosen to investigate the performance of the co-
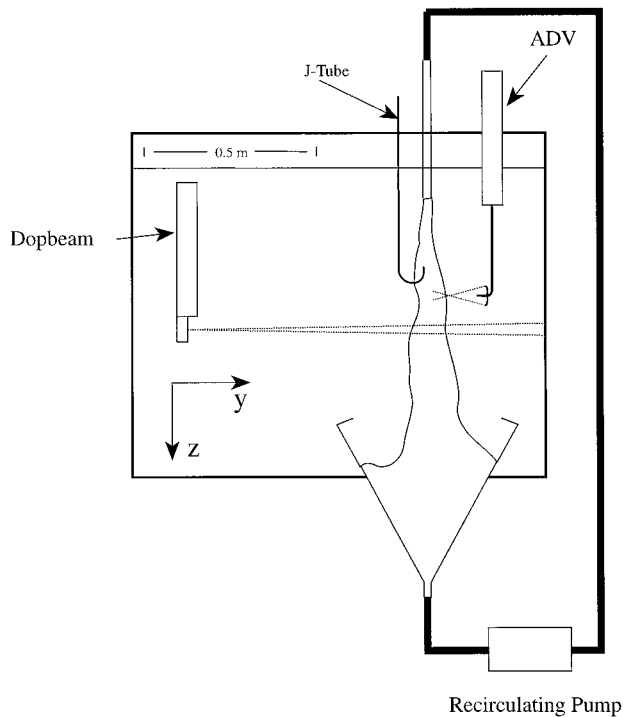
FIG. 2. Schematic diagram of the test tank facility identifying the position of the turbulent jet and relative placement of the instrumentation. The Dopbeam sampling beam is indicated by dotted lines projecting across the jet. The ADV point sample is indicated by the intersection of two dotted lines extending from the instrument's sampling probe. The ADV and Dopbeam have been offset for clarity but observations used for comparison were made at the same level in the jet. The J tube was removed from the jet during the acoustic measurement runs.

FIG. 3. Sketch showing the jet and the acoustic beam in horizontal cross section. Here β is the -3 dB angular width of the acoustic beam, $1.5°$ in our case. The shaded region is the detected volume at the jet centerline, u is the azimuthal velocity, and v the radial velocity. The 2-cm radius circles represent the jet.

herent Doppler profiler in a well-studied turbulent shear flow: a round jet (see List 1982; Hussein et al. 1994). The purpose of this paper is to present the results of this investigation. The experiments were carried out in a particle-laden jet using natural sand with a nominal median diameter of 180 μm. Thus, it is possible to present results not only on particle velocities, but also on particle concentrations and fluxes. These are of interest in themselves as there have been relatively few direct measurements of particle flux in turbulent two-phase flows. It is important to note as well that the scale width of the jet is about 2 cm, similar to the expected scale height of the wave boundary layer.

Pure momentum jets have been extensively studied (see, e.g., Fischer et al. 1979; List 1982). The behavior of suspended particles in turbulent jets has received less attention, and much of this has been more recent (Shuen et al. 1985; Parthasarathy and Faeth 1987; Chung and Troutt 1988). The velocities observed by the Doppler technique are not those of the fluid itself but rather they are the velocities of the particles suspended in the fluid. While this characteristic of the instrument is ideal for making particle flux measurements, it raises the question of the extent to 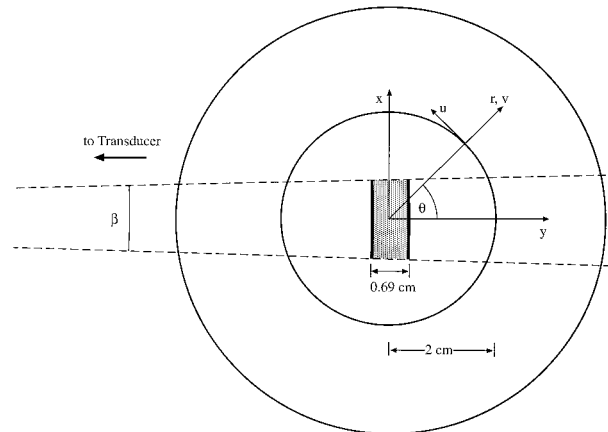which the particle velocities represent fluid motions. In particular, when turbulent motions are present, there is the potential that the suspended particles do not respond to the short timescale motions. This has possible ramifications for sediment transport theory (see, e.g., Nielsen 1992).

This paper is organized as follows. Apparatus and methods are summarized in sections 2 and 3. The results of the jet experiments are presented in three sections. Section 4 covers the (time mean) first moments: profiles of mean concentration and radial velocity; section 5 gives the second moments, the velocity, and concentration fluctuations; section 6 gives the cross-moments and the particle fluxes. Section 7 is a discussion of pulse-pair decorrelation time and the effects of the particle inertial timescale and settling velocity on the turbulence velocities obtained from the acoustic sensor. Section 8 summarizes our conclusions.

2. Apparatus

The turbulent jet is operated in a rectangularly shaped test tank roughly 1.2 m on a side, as shown in the vertical section in Fig. 2; this test facility is the same as that described by Hay (1991). The jet is directed vertically downward into quiescent water from a submerged 2-cm diameter nozzle. Positioned directly below the discharge nozzle is a capture cone that keeps most of the sediment in the recirculation circuit; the intake for the recirculating pump system is at the cone apex beneath the tank. The measured exit velocity from the nozzle is 93 cm s^{-1} (giving a Reynolds number for the jet of 2×10^4). Figure 3 shows the jet and the acoustic beam in horizontal cross section. The circles at 2-cm radius intervals represent the jet. The shaded area bounded by the $1.5°$ full-width of the acoustic beam (the half-power points in the monostatic directivity pattern of the 2.5-cm diameter transducer; Zedel et al. 1996) and the 0.69-cm

half-width of the transmitted pulse represents the Doppler profiler's detected volume at the jet centerline. Similar 0.69-cm-wide range bins are distributed along the y axis but are not shown. Typically, the transducer was located 50 cm away from the jet centerline in these experiments, so that the jet was in the transducer far field.

The Doppler profiler (or Dopbeam) is a general purpose 1.7-MHz phase-coherent acoustic sounder (Zedel et al. 1996). For our application we have configured the system to operate as a pulse-to-pulse coherent sonar as described by Lhermitte and Serafin (1984): radial velocities are estimated by determining the time rate of change of phase from time-sequenced pulse pairs. Accuracy is ultimately limited by the length of time that backscatter from any given range bin remains coherent (aside from restrictions in processing accuracy determined by the system hardware). Random motions within the range bin and the advection of scatterers through the range bin act to decorrelate the acoustic signal (Newhouse et al. 1976; Newhouse et al. 1977; Cabrera et al. 1987; Lhermitte and Lemmin 1990; Zedel et al. 1996). The magnitude of these decorrelation effects can be minimized by decreasing the time between pulses, but there are practical limits on the minimum pulse-pair separation, imposed by range and velocity ambiguities.

The ambiguities in coherent Doppler systems have been discussed by Brumley et al. (1990). The localized nature of the acoustic scatterers in the jet largely eliminate the range ambiguities (although reflections off the tank walls do cause problems and were avoided by adjusting the pulse–pulse separation). Similarly, the ambiguity velocity was chosen to be sufficiently large that it does not interfere with the present observations. Details of the signal processing employed by the Dopbeam system are presented in Zedel et al. (1996). Typical operating parameters allow profiling to a range of 1 m with 0.69-cm range resolution and a velocity uncertainty of 0.5 cm s^{-1} at a rate of 25 profiles s^{-1}.

A high quality velocity measurement system was required to serve as a reference for the Dopbeam velocities. For this purpose, we employed a Sontek acoustic Doppler velocimeter (ADV). The ADV is a single-point, three-component velocity measurement device. The 10-MHz acoustic pulses are transmitted by a central transducer, and backscatter from the (approximately) 1-cm^3 sample volume is detected by three inclined receiver beams. The location of the sample volume is approximately 10 cm in front of the central transducer so that the instrument is essentially noninvasive, as far as measurements in the jet are concerned. The Doppler shifts for the three received signals allow the three Cartesian velocity components in the sample volume to be determined. For the operating configuration reported here, the manufacturer reports a velocity accuracy of 1% for the maximum speed setting used in these experiments (100 cm s^{-1}). The ADV sampling frequency was 25 Hz.

Both the ADV and the Dopbeam rely on acoustic backscatter to provide a signal from which to determine velocities. Although the backscatter amplitude is itself not important to the velocity measurement, adequate signal levels are required to overcome electronic and thermal noise in these acoustic systems. For the present series of tests, particle concentrations adequate to provide a signal for the 1.7-MHz Dopbeam system would in general also provide an adequate signal for the 10-MHz ADV. We have chosen to use sand particles as acoustic scatterers because of our interest in making observations of suspended sand transport in the ocean. Measurements were made using beach sand with typical (centerline) concentrations of 1 g L^{-1} and ranging in diameter from 90 to 300 μm (the mean diameter was about 180 μm). The backscatter amplitude from particles is determined by the value ka, where k is the wavenumber and a is the particle radius (see, e.g., Hay 1991). For a given concentration, backscatter peaks at $ka \simeq 1$. At 1.7 MHz, ka ranges from 0.3 to 1.1 for our sand grain sizes. Note that 1 g L^{-1} corresponds to a volume concentration of less than 0.1%, low enough that multiple scattering is unlikely to have been important in these measurements.

One purpose of the jet experiments was to test the capability of the Dopbeam to resolve turbulence. With Nyquist frequencies of 12.5 Hz for the ADV, and 13.5–25.5 Hz for the Dopbeam (see below), the kinetic energy spectrum of turbulence in the jet is only partly resolved. Additional turbulence data were acquired using a TSI hotfilm anemometer. A TSI general purpose cylindrical probe (model 1210-20W) was selected; this platinum film on quartz substrate probe has a length of 0.51 mm and a diameter of 25.4 μm in the sensing zone. For comparison with these dimensions, the detected volume of the Dopbeam at the jet centerline in these experiments was 0.69 $\times$ 1.5 cm (Fig. 3), and for the ADV, 0.6 $\times$ 0.9 cm (as reported by the manufacturer). The hotfilm signal was digitized at 500 Hz, with 12-bit resolution.

3. Experimental procedure

The Dopbeam axis was directed horizontally across the jet and so sampled transverse velocities (see Fig. 2). For the various tests presented here, observations were made at 37.4 and 40 cm below the discharge nozzle. Pulses of 9.3 μs duration were transmitted at intervals of 930 μs, giving an ambiguity velocity of $\pm$23 cm s^{-1} and a range ambiguity of $\pm$0.69 m. For most of the data presented here, the range bin width and spacing was 0.69 cm. For these runs, averages over 5 or 10 pulses were evaluated to produce profiles at a rate of 51 or 27 s^{-1}, respectively. To produce data with higher velocity accuracy, one series of tests was collected with averages over 25 pulses while still retaining a profile rate of 27 s^{-1} by increasing the spacing between range bins to 1.05 cm. (The range bin width remained 0.69 cm for these runs.)

Runs were made with the ADV at several positions

across the jet in order to obtain ADV measurements for comparison with those of the Dopbeam and with the expected theoretical axial velocity profile, which the Dopbeam did not measure. In the jet, centerline velocities below the nozzle vary with distance (z) as (Fischer et al. 1979)

$$W(z) = 6.2W_0\frac{d}{z}, \qquad (1)$$

where d is the nozzle diameter and W_0 is the exit velocity. Equation (1) is valid for $z \gg l_q$, where l_q is a characteristic length scale determined by the volume and specific momentum transports at the nozzle; for round jets,

$$l_q = \sqrt{\pi/4}d, \qquad (2)$$

and this equals 1.7 cm for the present system. Defining $y = 0$ at the jet axis (Fig. 3), observations were made at 1-cm intervals from $y = -2$ cm to $y = 14$ cm. Data were collected at each position for 1 min at a level 37 cm below the discharge nozzle. The centerline axial velocity measured by the ADV at the 37-cm position was 30.3 cm s^{-1}, which compares favorably with the value of 31.2 cm s^{-1} predicted by Eq. (1). The axial velocities are at least an order of magnitude larger than the mean radial velocities so that even small alignment errors can lead to substantial biases in the radial velocity estimates. For the flux measurements, alignment of the Dopbeam to within 0.5° of horizontal was achieved by means of a spirit level mounted on the transducer case.

The Dopbeam backscatter signal was calibrated to provide quantitative measurements of suspended sediment concentration using the procedure described in detail by Hay (1991). The turbulent jet was operated with various quantities of sediment added to the system. Centerline concentrations were measured directly by drawing 1-L suction samples with the J-tube assembly (see Hay 1991). Three J-tube samples were drawn in rapid succession immediately after each acoustic data run. The concentration was determined from the volume of water drawn with the sample and the dry weight of the sand. The standard deviation of the concentrations determined from the three samples was typically 10% of the mean. Figure 4 shows the results for centerline backscatter amplitude as a function of centerline concentration, where analog to digital (A/D) counts represent the backscatter amplitude. Dots surrounding each data point in Fig. 4 indicate error bounds. For the concentration values, error bounds are ±1 standard deviation of the J-tube samples. Uncertainty for the receiver counts is based on the standard deviation of 4000 recorded acoustic backscatter samples taken from the jet axis. Because of the processing scheme we employ, each of these receiver counts represents the average over 10 acoustic transmissions. In Fig. 4, the concentration values are plotted on a logarithmic scale, while the counts are plotted on a linear scale because a logarithmic amplifier is used in the Dopbeam receiver. By fitting a straight line through
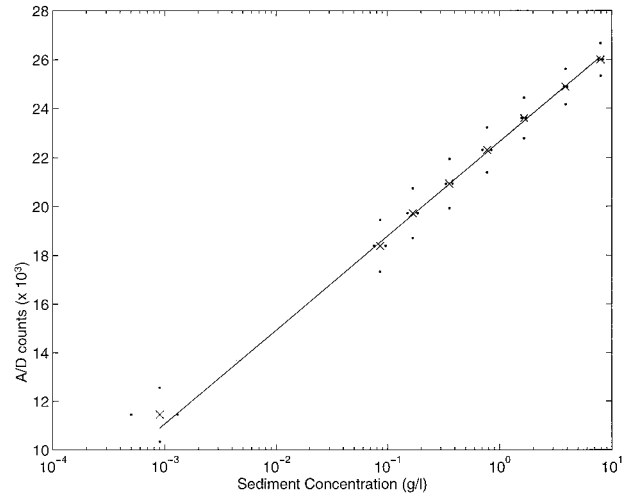

FIG. 4. Dopbeam receiver counts occurring at the axis of the jet plotted as a function of J-tube determined, sediment concentrations. A regression fit straight line is shown. Error bounds (±1 standard deviation) are indicated by dots surrounding data points.

the data, recorded A/D counts can be related to jet centerline concentration as

$$m = (3856 \pm 61.7)\log_{10}(C) + (226\,40 \pm 41), \quad (3)$$

where C is the measured sediment concentration in grams per liter. The calibration constants given in Eq. (3) provide an estimate of sediment concentration with an uncertainty of less than 10% for concentrations between 0.001 and 10 g L^{-1}.

4. Results I: Mean profiles

In this section we present results for the mean suspended sediment concentrations and velocity across the jet, and compare these results to previous measurements and to entrainment-based theories of round jet behavior.

a. Mean concentration and axial velocity

The profile of mean concentration across the jet is shown in Fig. 5. There is reasonably good overall agreement with the expected Gaussian form, shown by the dashed line. The transverse profile of mean axial velocity W measured with the ADV is shown in Fig. 6. The dashed line is a Gaussian fit. As with the mean concentration profile, the data are reasonably well represented by the Gaussian form. The width at half-maximum of the axial velocity is less than that of the concentration profile. Note that this is opposite to what is seen with passive scalars (Fischer et al. 1979) but consistent with previous results for negatively buoyant particles in downward-directed vertical jets (Popper et al. 1974; Hay 1991). Hay (1991) showed that this narrowing of the jet can be explained as a settling velocity effect.
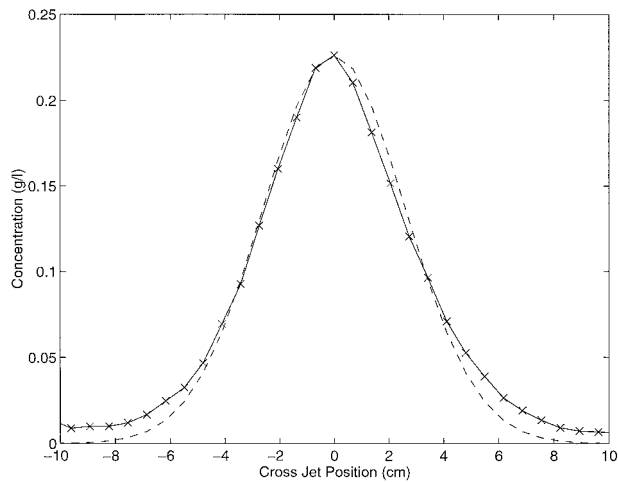
FIG. 5. Profile of mean suspended sediment concentration across the jet (×'s joined by a solid line). The dashed line indicates the Gaussian form expected for the concentration profile [Eq. (13)]: b_c for the fit is 0.065.

FIG. 6. Profile of measured mean axial velocity W across the jet (×'s). The dashed line indicates a Gaussian fit to the measurements [Eq. (4)]: b_w for the fit is 0.094.

b. Mean transverse velocity

Figure 7 shows the time-averaged transverse velocity V as a function of position y across the jet, measured with the Dopbeam (solid line), and the ADV (×'s). Both sets of measurements show a mean outward divergence from the core of the jet. Peak radial velocities in the ADV and Dopbeam data are both about 1.25 cm s^{-1}, occurring at a radius of 3–4 cm. For $y > 5$ cm, the ADV data suggest a somewhat broader jet. Beyond $y = \pm 8$ cm from the jet axis, there is a mean inward convergence (associated with entrainment; see next section), which is better resolved in the Dopbeam data. The ADV velocities tend to be noisy toward the edge of the jet. The bad data in this region coincide with sporadic low pulse-pair correlations even while adequate signal levels are received.

Also plotted in Fig. 7, as open circles, are laser Doppler anemometer (LDA) observations made in a particle-laden, turbulent water jet by Parthasarathy and Faeth (1987), rescaled by our observed centerline velocity to recover dimensional values. While both sets of observations show the same form for the velocities, those of Parthasarathy and Faeth are larger by a factor of about 1.5. Reasons for this difference are not immediately obvious, as the LDA also specifically senses particle velocities. Parthasarathy and Faeth used a 0.5-cm diameter discharge orifice, an exit velocity of 161 cm s^{-1}, and 500-μm diameter glass spheres. The open circles in Fig. 7 are their measurements of the radial velocities of these large particles (smaller natural seed particles were used to sense the fluid velocity). Because their mean particle concentrations were large (2.4% and 4.8% by volume compared to a maximum of 0.1% in the present data), Parthasarathy and Faeth computed concentration-weighted averages. Thus, these velocities asymptote to a nonzero positive velocity at large
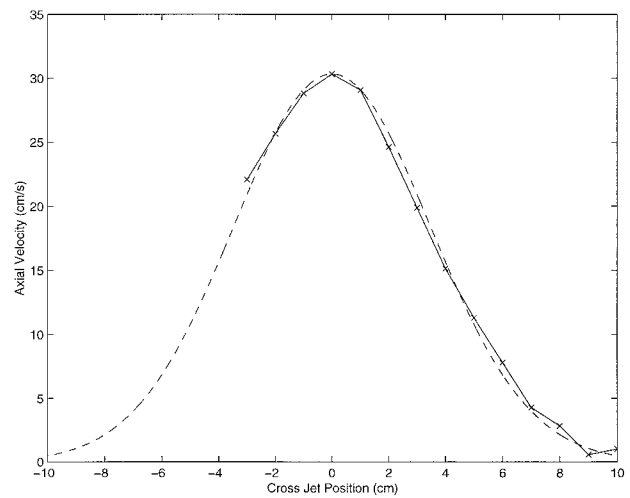
y, since the inward-moving ambient fluid carrying the small seed particles did not contribute to the average.

The measured transverse velocities can also be compared to the accepted form for turbulent round jets (Fischer et al. 1979). The axial velocity W is given by

$$W = \frac{W_k}{z} \exp\left(\frac{-r^2}{2b_w^2 z^2}\right), \tag{4}$$

where z is the distance from the jet nozzle, $W_k = 6.2W_0 d$ with $W_0 = 93$ cm s^{-1} being the nozzle exit velocity, r is the radial distance from the jet axis, and b_w is an experimentally determined width parameter (from Fischer et al. 1979; $b_w = 0.076$). From the continuity
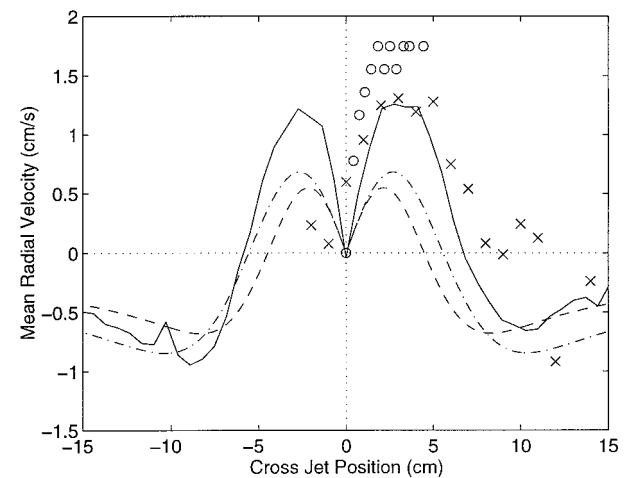

FIG. 7. Jet radial velocities at a position 37 cm below the jet nozzle. Mean radial velocity measured by the Dopbeam (solid line), and the ADV (×'s). Laser Doppler observations presented by Parthasarathy and Faeth (1987) are indicated by circles, and the dashed line and the dashed–dot line are derived from assuming a Gaussian velocity profile [Eq. (5)] with $b_w = 0.076$ and $b_w = 0.094$, respectively.

relation in cylindrical coordinates and Eq. (4), one obtains the following relation for the mean transverse velocity V:

$$V = \left[\left(1 + \frac{r^2}{b_w^2 z^2} \right) \exp\left(\frac{-r^2}{2b_w^2 z^2} \right) - 1 \right] \frac{W_k b_w^2}{r}. \quad (5)$$

The radial velocities predicted by Eq. (5) for $b_w = 0.076$ are indicated by the dashed line in Fig. 7. Near the jet axis, the magnitude of the prediction is smaller than the Doppler profiler results. In the entrainment-driven convergence region beyond 10-cm radius, the Doppler profiler measurements match the predictions quite well. The dot–dashed line is the prediction for $b_w = 0.094$, the value obtained from the fit in Fig. 6. Increasing b_w leads to improved agreement with the Doppler profiler in the core region of the jet, particularly for the first off-axis zero crossing in V. It can be seen from Eq. (5) that the term in square brackets controls the zero crossings and is quite sensitive to the shape of the velocity profile (i.e., b_w). The larger value of b_w increases the first radial velocity maximum slightly, but this value remains roughly a factor of 2 smaller than the value indicated by the profiler and ADV data. The width parameter b_w cannot be made much larger without affecting the entrainment estimates (see below).

c. Entrainment

The present measurements can also be evaluated against the accepted velocity form given by Fischer et al. (1979) by comparing entrainment rates. The divergence of the total axial fluid transport Q is determined by the total inward transport across a circle of radius r outside the jet and centered on the jet axis:

$$\frac{dQ}{dz} = -2\pi r V. \quad (6)$$

The magnitude of the right-hand side of this equation is the entrainment rate E. From Eq. (5) for large values of r and $b_w = 0.076$, it can be shown that

$$E = 0.25 \frac{Q_0}{l_q}, \quad (7)$$

where $Q_0 = 2.92 \times 10^{-4}$ m^3 s^{-1} is the initial volume transport of the jet, and $l_q = 1.77 \times 10^{-2}$ m [from Eq. (2)]. These values give $E = 4.12 \times 10^{-3}$ m^2 s^{-1}, the predicted entrainment rate.

We can determine the jet entrainment rate from the acoustic Doppler measurements by interpreting the values of V at about 10 cm from the jet axis as the entrainment velocity. From the near side of the jet (the side closest to the transducer), we get $E = 5.1 \pm 0.8 \times 10^{-3}$ m^2 s^{-1} and from the far side we get a value of $3.6 \pm 0.4 \times 10^{-3}$ m^2 s^{-1} (here the uncertainty is the standard deviation of four separate observations). The asymmetry is due to the proximity of the tank wall on the far side of the jet. In the x–y plane, the entrainment

field can be modeled as a potential flow sink at the jet axis: this sink is imaged in the tank wall. The radial velocity along the $x = 0$ axis becomes

$$V = \frac{E}{2\pi y} \left(1 - \frac{y}{2L - y} \right), \quad (8)$$

where L is the distance from the jet centerline to the tank wall (34 cm). The second term is due to the image sink. Substituting the measured radial velocities at $y = \pm 10$ cm gives $E = 4.5 \times 10^{-3}$ m^2 s^{-1} on the near side of the jet and 4.4×10^{-3} m^2 s^{-1} on the far side. The average of all observations, accounting for the wall effect, gives an entrainment rate of $4.4 \pm 0.6 \times 10^{-3}$ m^2 s^{-1}, in agreement with the value of 4.12×10^{-3} m^2 s^{-1} obtained from Eq. (7).

5. Results II: Fluctuations

In this section we consider the behavior of velocity and concentration fluctuations across the jet. As Fig. 8 illustrates, the fluctuations detected by the Dopbeam are large and span a range of scales. This figure also suggests that the larger-scale fluctuations in concentration and velocity are coherent, a point pursued in the next section.

a. Velocity standard deviations

Figure 9 shows transverse profiles of the radial velocity standard deviations for the Dopbeam (dashed line). The experiment runs are the same as for Fig. 7. Following Hussein et al. (1994), the standard deviations are normalized by the jet axial velocity and radial position is normalized by the distance from the discharge nozzle.

The Dopbeam profile has the same form as that obtained by Hussein et al. (1994) for a pure momentum jet (indicated by the solid line in Fig. 9), but the magnitudes are smaller (by about 30% at the jet centerline). The fluid velocity observations of Parthasarathy and Faeth (1987) from a particle-laden (water) jet are indicated by $\times$'s: their fluid velocity measurements are closer to those of Hussein et al. at the centerline but fall off more rapidly with radial distance. The particle velocities obtained by Parthasarathy and Faeth (1987) at the centerline are quite comparable to the Dopbeam. Away from the centerline, their particle velocity variance tends to remain constant, in contrast to the fluid velocity variance and the Dopbeam velocity variance. (Their particle velocities do, however, appear somewhat noisy).

Centerline turbulence intensities depend not only upon local axial velocity, but also upon distance from the nozzle. Our measurements were made 20 nozzle diameters along the axis. According to Fischer et al. (1979, p. 322), this should be well within the zone of fully established flow. However, List (1982) has shown
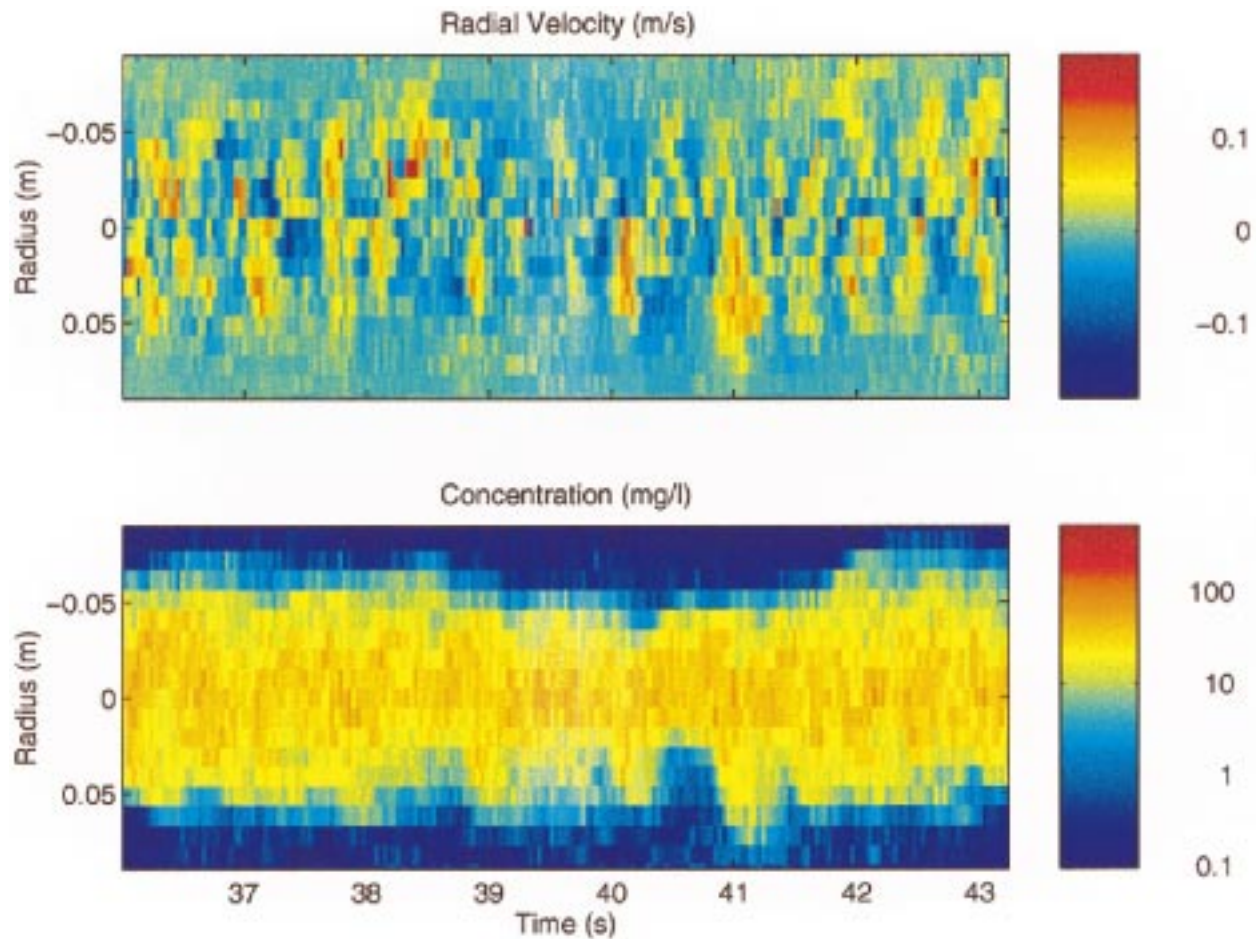
FIG. 8. Sample (a) jet radial velocity and (b) concentration profiles taken across the turbulent, particle-laden jet. Displayed are 17 s of data; the y axis indicates distance from the jet axis. The data are 25-ping averages, with a 1.05-cm range bin interval.

on the basis of the available measurements that the turbulence fields become self-preserving only at downstream distances greater than about 40 nozzle diameters. In this region, the radial velocity standard deviation at the centerline equals $0.23W_m$, where $W_m = W_k/z$ is the local mean axial velocity at the centerline. Hussein et al.'s measurements are consistent with this result. The Dopbeam value at the centerline is about $0.16W_m$, 30% less. List's (1982) summary of previous experiments indicates that at 20 nozzle diameters distance, the axial velocity fluctuations w' show a 20% reduction in centerline standard deviation compared to the fully developed, self-preserving region of the jet farther downstream. Assuming similar behavior for v' and w', adjustment of our $(v'^2)^{1/2}/W_m$ data brings our centerline value to within 10% of the pure momentum jet results.

The shapes of the profiles in Fig. 9 are of interest. The smooth variations in turbulence intensity with r/z in the Dopbeam results are quite comparable to the laser Doppler velocimeter (LDV) fluid velocity measurements of Hussein et al., a pleasing result. The particle velocities measured by Parthasarathy and Faeth behave

differently. Their particle velocities are based on averages of instantaneous measurements of single large (500-μm diameter) particles transiting the 600×700 μm detected volume of their LDV. Our measurements represent averages over many more particles in a larger detected volume. Parthasarathy and Faeth also used much higher mean particle concentrations in their experiments and therefore performed a concentration-weighted average of their velocities.

Included for completeness in Fig. 9 are the ADV data (dotted line). Near the jet centerline, the transverse velocity variances obtained with the ADV are comparable to the Dopbeam values (within 13% at the centerline). However, the ADV variances are significantly greater at radial distances of about 4 cm or more ($r/z = 0.1$). We do not know the cause of increased variance in this region but note that it was associated with low signal correlations.

b. Kinetic energy spectra

Figure 10 shows a comparison between kinetic energy spectral densities obtained with the hotfilm and the Dop-
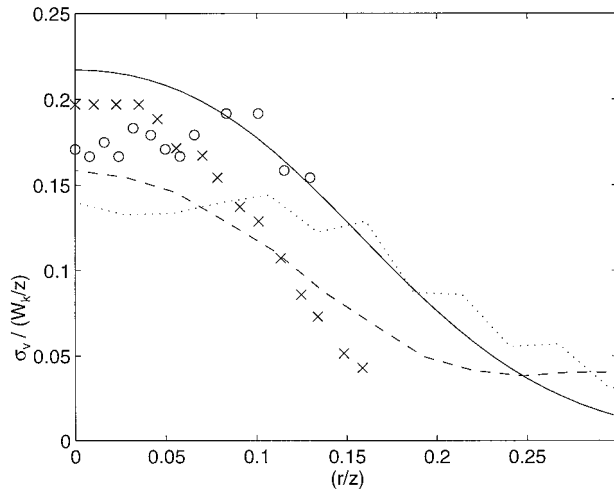
FIG. 9. Standard deviation of transverse velocity fluctuations across the jet at a position 37 cm below the jet nozzle; the dashed line indicates Dopbeam observations, dotted line indicates ADV observations, solid line indicates LDV observations of Hussein et al. (1994), circles indicate particle velocities observed by Parthasarathy and Faeth (1987), and crosses indicate fluid velocities observed by Parthasarathy and Faeth (1987). Data have been normalized by centerline axial velocity and the x axis has been normalized by distance from the nozzle.
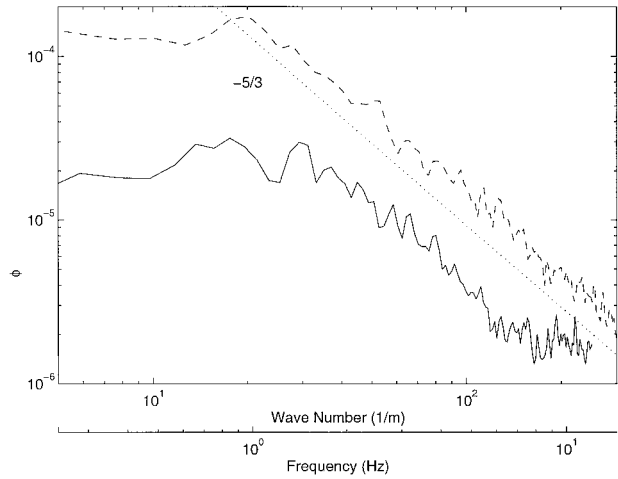

FIG. 10. Example of turbulent spectra observed at the jet axis 40 cm from the nozzle. The solid line indicates Doppler velocity estimates, transverse to the jet, data averaged over 25 acoustic transmissions. The dashed line represents hotfilm anemometer data (essentially measuring jet axial velocity) sampled at 500 s^{-1}. The dotted line indicates a $-5/3$ spectral slope.

beam at the jet centerline. Taylor's frozen field hypothesis (e.g., Tennekes and Lumley 1972) has been invoked to transform time domain measurements to wavenumber space using the relationships

$$\phi(k) = \frac{\phi(f)}{2\pi/W} \qquad (9)$$

and

$$k = \frac{2\pi f}{W}, \qquad (10)$$

where ϕ is the one-dimensional kinetic energy spectral density, W is the mean axial velocity at the sample point, and k is the wavenumber.

The Dopbeam spectrum (indicated by the solid line) was obtained using averages over 25 pulse transmissions producing average profiles at a rate of 24.1 s^{-1}. The spectrum measured using the hotfilm anemometer is indicated in Fig. 10 by the dashed line. The straight dotted line indicates the $-5/3$ spectral slope characteristic of the inertial subrange. Both the hotfilm and the Dopbeam spectra exhibit a $-5/3$ region.

The general form of the hotfilm and Dopbeam energy spectra shown in Fig. 10 are in agreement, but the hotfilm spectral densities are greater than those of the Dopbeam by a factor of about 3.5. The hotfilm measurements are the jet axial component of velocity while the Dopbeam measured the jet radial component, a potential source of disagreement. Comparison between the ADV and the Dopbeam observations from the jet centerline

are shown in Fig. 11. In Fig. 11 Dopbeam data, sampled at 27.7 s^{-1}, are indicated by the solid line; and the ADV data, sampled at 25 Hz, are indicated by a dashed line for axial velocities and a dash–dot line for radial velocities. A $-5/3$ slope is indicated by the dotted line. The ADV axial velocities indicate more energy at low wavenumbers, but the inertial subrange for all spectra are the same and the ADV radial velocities agree extremely well with the Dopbeam (radial) velocities.
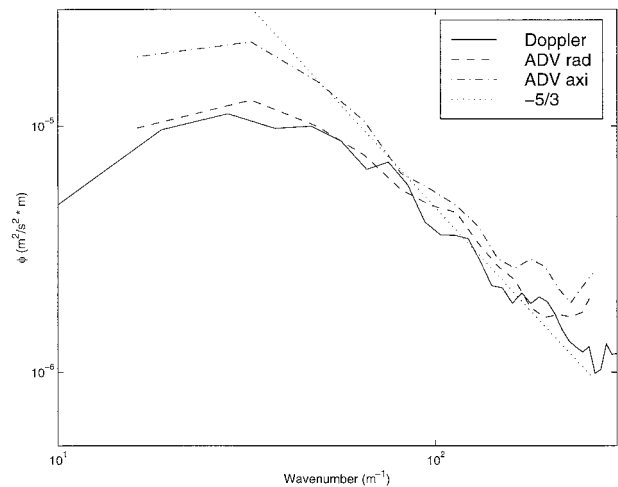

FIG. 11. Turbulent spectra observed at the jet axis 40 cm from the nozzle. The solid line indicates Doppler velocity estimates; the dashed and dash–dot line indicate ADV axial and radial velocities, respectively. The dotted line indicates a $-5/3$ spectral slope. The system configuration is similar to that shown in Fig. 10 but the datasets were collected at different times and so cannot be compared directly.
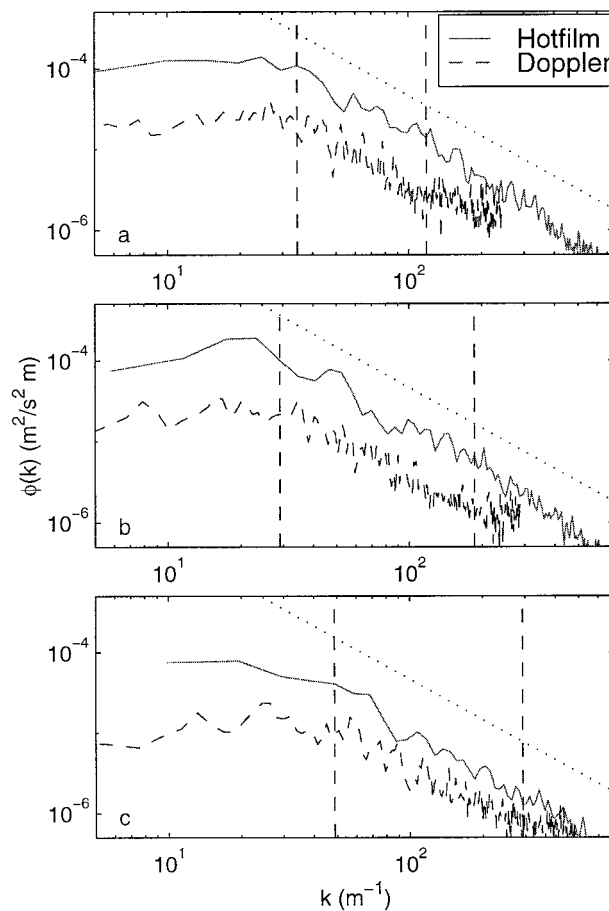
FIG. 12. Turbulent spectra at different values of y: (a) on axis, $y = 0$; (b) 2 cm; and (c) 3 cm.

FIG. 13. Profiles of mean (solid line), maximum ($\times$'s), and minimum ($\times$'s) concentration across the jet. Concentration values are normalized by axial concentration; cross jet position is normalized by distance from the nozzle. Data shown are averaged over 25 acoustic transmissions.

onstrating the general form of the energy spectra because of the much greater spectral resolution it provides.

Figure 12 shows hotfilm and acoustic Doppler spectra at several positions across the jet. All locations show a well-defined $-5/3$ inertial subrange. There is a shift of the inertial subrange toward higher wavenumbers with increased distance from the jet centerline.

In Fig. 10, the Dopbeam spectrum flattens out at wavenumbers greater than 200 m^{-1}. As mentioned previously, the acoustic beam has a width of about 1.5 cm at the sample point: this length defines the spatial resolution limit of the system and corresponds to a wavenumber of $2\pi/(2 \times 0.015 \text{ m}) = 210 \text{ m}^{-1}$. This wavenumber is in the vicinity of the apparent noise floor in Fig. 10. One would expect the spatial resolution limit to average out smaller-scale fluctuations and thus increase the spectral rolloff. That this does not happen suggests the possibility of aliasing. Aliasing can occur in our system because of dead time between sample bursts: for a given ensemble-profile repetition rate, this dead time is reduced when the burst contains more pings.

c. Concentration fluctuations

Consistent with measurements of passive scalar concentrations in turbulent jets, the sonar reveals large-amplitude fluctuations in suspended particle concentration. Figure 13 shows the mean, maximum, and minimum concentrations observed across the jet (normalized by the jet centerline concentration). These data have been averaged over 25 transmissions. The maximum centerline value shows a normalized concentration of about 3; the normalized standard deviation here is about 0.35. Both of these values are consistent with the peak

Hussein et al. (1994) found that turbulence in axisymmetric jets is not isotropic: at the centerline position, they report a normalized variance of 0.076 for axial velocities measured with a stationary hotfilm anemometer, compared to 0.047 for the radial velocity variance measured with an LDA. For the observations shown in Fig. 11, the normalized variance in radial measurements is 0.036 (ADV), and 0.028 (Dopbeam) compared to 0.056 for the ADV axial measurements. Here again, we note that our observations are not strictly in the self-preserving region of the jet and could be low by about 20% (List 1982). If we correct our observations for this difference, the normalized variance becomes 0.056 (ADV radial), 0.044 (Dopbeam radial), and 0.091 (ADV axial). These values compare very favorably with the observations by Hussein et al. (1994). In contrast, the hotfilm obervations shown in Fig. 10 indicate a normalized variance of 0.104 (which corrects to a value of 0.16), which is clearly inconsistent with the other observations. From these results we conclude that the hotfilm system cannot be used for quantitative comparisons in the present studies. It is, however, valuable in dem-
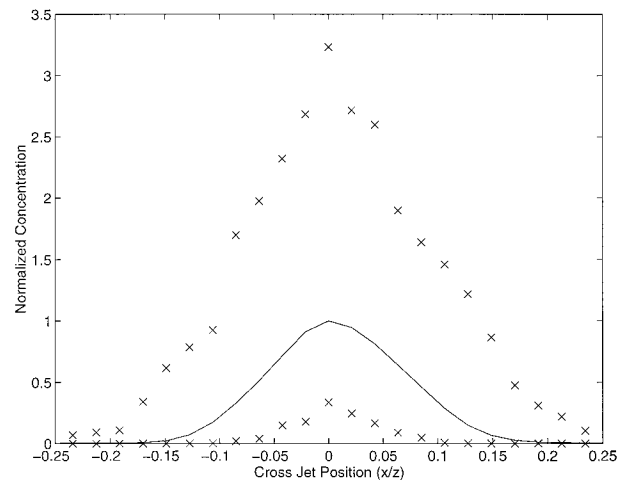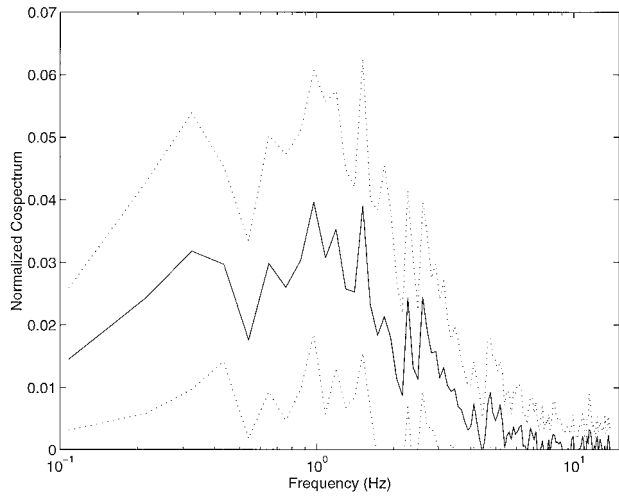
FIG. 14. Real component of the cross–spectrum between radial velocity and sediment concentration fluctuations normalized by the total cross-spectral variance at a point 2 cm from the jet axis. The dotted lines indicate 95% confidence intervals.

centerline value of 2.3 and standard deviation of 0.34 reported by Papantoniou and List (1989) for the concentration of a passive scalar (fluorescein dye) in a turbulent round jet.

Note that when the backscatter data are averaged over fewer acoustic transmissions, the apparent variability in particle concentration estimates increases. This is a result of configuration (or speckle) noise, caused by the phase superposition of waves scattered from individual particles in random relative motion. For example, for data where averages are formed over only 10 transmissions, the on-axis (normalized) standard deviation increases to 1.0. For the Dopbeam, successive acoustic transmissions do not represent independent samples of the scatterer population by definition, since the returns from consecutive pulse pairs must remain phase coher-

ent in order to estimate velocities. Thus, these averages include a coherent component.

6. Results III: Suspended sediment fluxes

The time-averaged radial sediment flux is given by

$$\overline{F} = \overline{vc} = VC + \overline{v'c'}, \tag{11}$$

where primed variables indicate the turbulent components and time-averaged quantities are indicated either by an overbar or upper case.

Provided the velocity and concentration fluctuations are correlated, the turbulent radial particle flux $\overline{v'c'}$ will be nonzero. Figure 14 displays the radial velocity and concentration cospectrum at a point 2 cm from the jet axis. The cospectral densities are significantly different from zero at frequencies less than about 4 Hz, indicating that the radial particle flux occurs predominantly below this frequency. There is a broad peak in the cospectrum at about 1 Hz. The mean axial velocity 2 cm from the jet axis is about 23 cm s^{-1}, so the 1-Hz frequency corresponds to an eddy scale size of 12 cm or to a wavenumber of 27 m^{-1}. From Fig. 10, this frequency and wavenumber lie well outside the inertial subrange, corresponding instead to the large eddy turbulent production scales.

Figure 15 shows the low-pass filtered radial particle flux as a function of time and transverse position. This picture is dominated by large-scale eddies advecting particles from the centerline region outward. At $y = 2$ cm, these flux structures appear at a frequency of about 1 Hz, consistent with the cospectrum. Such dominance of the particle flux by large-scale structures is not unexpected, either for particle-laden jets or any other particle-transporting shear flow. The size of these structures in the axial direction, estimated from the 23 cm s^{-1} axial speed and their approximate 1-s duration (Fig. 15), is a few centimeters. This scale size is roughly the half-width of the jet, as expected. Comparing Fig. 15 with
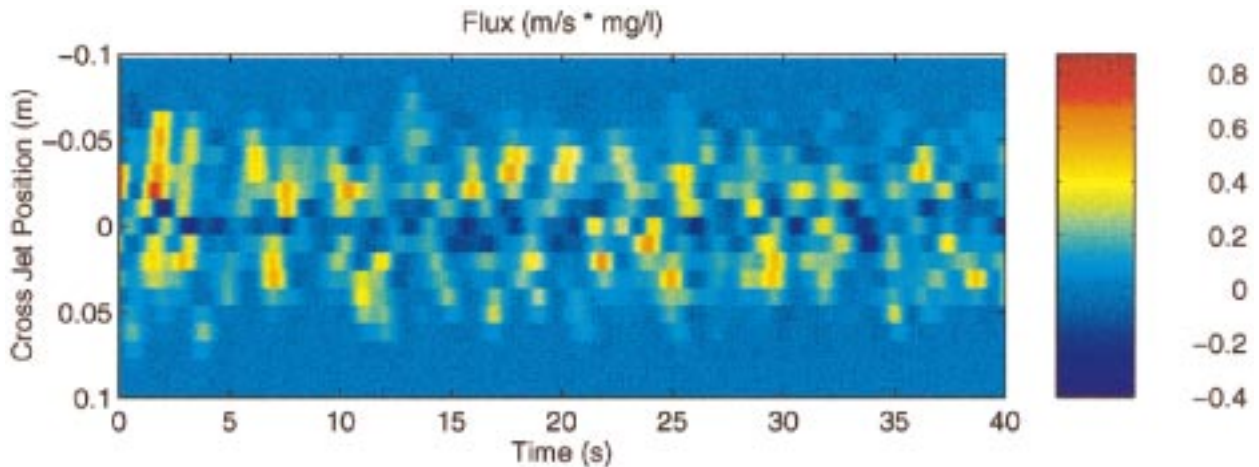

FIG. 15. Color image of radial particle flux 40 cm from the nozzle. Same data as in Fig. 8.

Fig. 8, it can be seen that the flux structures are usually related to outward-bound particle-laden ''plumes,'' which are preceded and followed by inward-bound clear water plumes: thus, the time–space structure of the flux image at these larger scales is consistent with the coherent structure picture of large-scale turbulence (e.g., McComb 1990).

Figure 16 shows the cross-jet profiles of the different contributions to the radial particle flux. The mean flux VC is indicated by the dotted line. The mean turbulent flux $\overline{v'c'}$ is indicated by the dash–dot line. These profiles peak at a y position of about 2 cm, roughly the position of maximum gradients in mean concentration (Fig. 5) and in mean axial velocity, from Eq. (4), where maximum production is expected. The peak turbulent flux is less than half the peak mean flux. The total observed radial flux is indicated by the solid line.

For both Figs. 14 and 16, data were averaged over 10 pulses. From the previous discussion of concentration fluctuations in the jet, we know that this amount of averaging is insufficient to eliminate the configuration noise from the instantaneous concentration estimates at the profile acquisition rate. However, interference-induced amplitude fluctuations ought to be uncorrelated with velocity (phase) fluctuations. Thus, such noise should be suppressed by averaging $v'c'$ over time.

There are no other direct measurements of radial particle flux in a turbulent jet of which we are aware, to which comparisons of the results in Fig. 16 might be made. However, it is possible to compare the measured mean radial transport profile to estimates formed from previous work on axial mean transports. The time-averaged particle flux is nondivergent. In cylindrical coordinates, neglecting the azimuthal flux terms because of symmetry, the radially integrated form of the time-averaged flux divergence can be written as

$$\frac{1}{r} \int r \frac{\partial}{\partial z} WC \, dr + VC + \overline{v'c'}$$
$$= -\frac{1}{r} \int r \frac{\partial}{\partial z} \overline{w'c'} \, dr, \quad (12)$$

where r is the radial coordinate.

All of the terms on the left-hand side of Eq. (12) can be evaluated from the acoustic Doppler measurements. The mean and turbulent radial flux terms, VC and $\overline{v'c'}$, are measured directly. The first term is the radial integral of the mean axial flux (WC) divergence, which we estimate using entrainment-based models. The axial velocity is given by Eq. (4). The mean concentrations shown in Fig. 5 have a Gaussian shape, which, as Shuen et al. (1985), Parthasarathy and Faeth (1987), and Hay (1991) have shown, can be approximated by

$$C = \frac{C_k}{z} \exp\left(\frac{-r^2}{2z^2 b_c^2}\right), \quad (13)$$
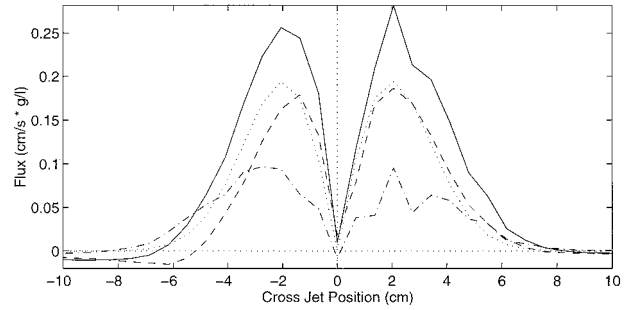

FIG. 16. Particle flux profiles across the jet at a point 40 cm below the nozzle for a centerline concentration of 0.22 g L^{-1}. The dotted line indicates observed mean radial flux VC; The dash–dot line indicates the observed turbulent flux $\overline{v'c'}$. The solid line is the total observed flux, the sum of VC and $\overline{v'c'}$. The dashed line is the computed mean axial flux divergence, multiplied by -1, the first term in Eq. (12).

where C_k/z is the centerline concentration and b_c is observed to be about 0.065 in the present data.

The negative of the first term in Eq. (12) is plotted in Fig. 16 as a dashed line: it has the same form and very nearly the same magnitude as the observed mean radial transport. Thus, the mean radial flux VC and axial mean transport divergence are essentially in balance. The mean turbulent radial flux $\overline{v'c'}$ is nearly 50% of VC at $y = 2$ cm, and a higher percentage at larger values of y. The axial turbulent transport divergence, the term on the right-hand side of Eq. (12), must therefore balance $\overline{v'c'}$.

7. Discussion

a. Correlations

Velocity estimates by coherent Doppler require phase coherence between successive pulse pairs. The most significant processes leading to decorrelation are scatterer advection through the beam and nonuniform particle motions in the sampling volume (e.g., turbulence). Cabrera et al. (1987) discuss these processes. We are interested here in the capability of the Dopbeam to resolve turbulent fluctuations, so a discussion of correlations is relevant.

For sampling in the turbulent jet, a first concern is the presence of a significant velocity transverse to the acoustic beam. The advection of particles through the beam causes decorrelation both because of geometrical effects and scatterer exchange with the surrounding fluid (Newhouse et al. 1976; Newhouse et al. 1977). This effect can be estimated for a given beam pattern (Zedel et al. 1996). For the present observations, the axial velocity is about 30 cm s^{-1}, and the pulse delay being used was $\tau = 930$ μs. These values imply a correlation coefficient (due to particle advection) of $R^2 = 0.971$ (see Zedel et al. 1996). The correlation coefficient and velocity variance (σ_v^2) are related by

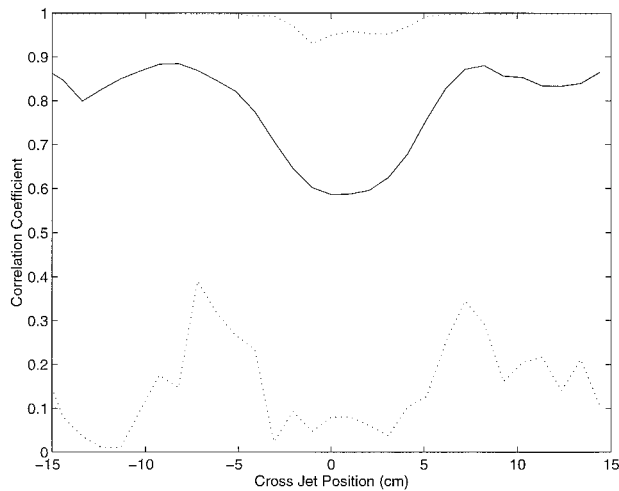$$R^2 = \exp(-8\pi^2 \tau^2 \sigma_v^2 / \lambda^2), \quad (14)$$

FIG. 17. Doppler pulse-pair correlation coefficient across the turbulent jet. Mean values are indicated by the solid line; the dashed lines above and below indicate the maximum and minimum correlations observed. The jet axis defines the cross-position origin.

FIG. 18. Decorrelation times determined using Eq. (14) for the mean correlation coefficients indicated in Fig. 17.

where λ is the acoustic wavelength (Zedel et al. 1996). For the system configuration used here, the correlation coefficient of 0.971 implies a velocity uncertainty of σ_v = 1.8 cm s^{-1} for a single pulse pair. When averaged over, for example, 25 estimates, velocity uncertainties of ± 0.36 cm s^{-1} would be expected.

In using Eq. (14) it is important to realize that signal correlation is limited by many factors including system operating parameters and the received signal-to-noise ratio. Equation (14) is only strictly applicable under those conditions when signal decorrelation is dominated by processes associated with scatterer motions. In the present application, these conditions are reasonably approached as demonstrated by the high correlation coefficients that can be observed in the present data.

An example of correlation coefficients observed 37 cm beyond the nozzle when the Doppler was operating with 930 μs between transmissions is shown in Fig. 17. For the mean correlation coefficients (solid line in Fig. 17), the minimum value occurs at the jet axis, consistent with our expectation of maximal turbulence and transverse velocities. The dashed lines in Fig. 17 indicate the maximum and minimum observed correlation coefficients. Very high correlation coefficients can occur when all particles in the sample volume have the same velocity or when there is only one (acoustically) dominant scatterer in the sample volume. For most positions across the jet, the maximum correlation coefficients are very close to unity except at the jet axis where maximum values of about 0.95 were observed. At the jet axis, the axial velocity contributes to signal decorrelation and so unity correlation coefficients would be unlikely. In addition, the high scatterer concentrations typical of the jet axis would reduce the possibility of a single scatterer dominating the signal. The observed maximum of 0.95 at the jet centerline is very close to the value of 0.97
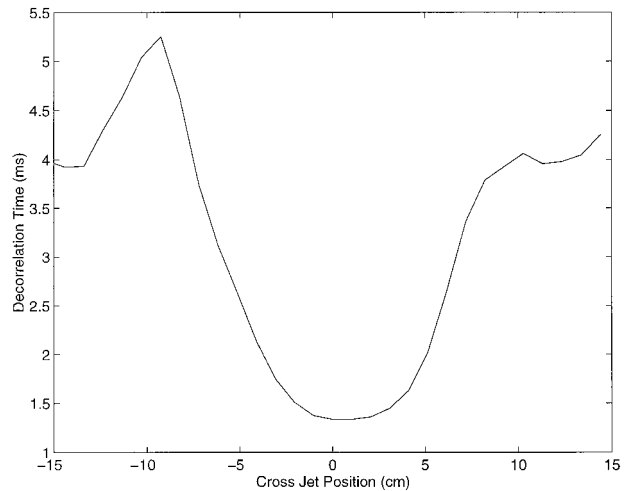
expected based on the beam geometry, operating parameters, and 30 cm s^{-1} axial velocity.

The lowest correlation coefficients fall between 0 and 0.4. Outside the jet, low signal levels (due to few scatterers) could contribute to the low correlations. Beyond the jet boundaries there is also the possibility of reflections from the tank walls contaminating the volume-scattered signal. Within the jet, low correlations are most likely a result of turbulent bursts contributing to both the turbulent decorrelation and the advection velocity.

While high correlation coefficients are important for accurate velocity estimates, they indicate a lack of independence between successive samples. Such independence is important when backscatter data are being averaged to obtain particle concentrations as noted in section 4a. The decorrelation time can be defined as the characteristic decay time of the correlation coefficient. From Eq. (14),

$$\tau_d = \lambda(2\sqrt{2}\sigma_v\pi)^{-1}. \qquad (15)$$

Using Eq. (14) σ_v can be estimated, and the corresponding values of the decorrelation time (τ_d) can be found using Eq. (15). For observations made at the 37-cm position (the same data used in making Fig. 17), the average decorrelation times at positions across the jet are shown in Fig. 18. Decorrelation times at the jet axis are about 1 ms and reach maximum values of between 4 and 5 ms outside the jet. In order for backscatter to be truly independent, the time between acoustic transmissions must be somewhat longer than the decorrelation time. From the values shown in Fig. 18, samples made at a rate of 500 s^{-1} (at a time interval of twice the decorrelation time) will be independent at the axis, while toward the edges of the jet, independent samples are only acquired at a rate of 100 s^{-1}. For the rate of acoustic transmissions being used for the present Doppler measurements (1075 transmissions per second), only

every other velocity estimate would be independent at the jet axis, while at the jet edges, independent samples would be acquired after collecting every 10th sample. Averaged profiles have only been produced at a rate no greater than 50 s^{-1} and so successive averaged velocity profiles will most certainly be independent.

b. Particle motion

Acoustic Doppler systems require that scatterers (particles in our case) be present in order to have a signal. The question arises as to how representative the particle velocities are of the fluid motions. The selection of particles for LDV flow measurement require consideration of this same problem (see, e.g., Buchhave et al. 1979). Whether a particle will behave as a passive tracer or not depends, in part, on its inertia (Snyder and Lumley 1971; Siegal and Pluedemann 1991). The characteristic particle response time is (Snyder and Lumley 1971)

$$\tau_p = \frac{W_s}{g}, \tag{16}$$

where W_s is the still-water particle-settling velocity and g is the acceleration due to gravity. Here W_s values for 100–300-μm diameter sand grains are in the 1–3 cm s^{-1} range (Sleath 1984), giving time constants of 1–3 ms.

These particle time constants can be compared to the Kolmogorov time microscale,

$$\tau_K = \left(\frac{\nu}{\epsilon}\right)^{1/2}, \tag{17}$$

where ν is the kinematic molecular viscosity and ϵ is the dissipation rate. Here τ_K sets an upper bound on the frequencies of turbulent velocity fluctuations (e.g., Tennekes and Lumley 1972). The energy dissipation rate can be estimated from the one-dimensional kinetic energy spectral density in the inertial subrange, using

$$\phi(k) = \alpha\epsilon^{2/3}k^{-5/3}, \tag{18}$$

where α is a constant with an approximate value of 0.5 (Tennekes and Lumley 1972). The Dopbeam spectral densities in Figs. 10 and 12 give inertial dissipation rates of 2.1×10^{-3} m^2 s^{-3} at the jet centerline and 2.3×10^{-3} m^2 s^{-3} at $y = 3$ cm. These dissipations give time microscales of 23 ms at the jet centerline and 22 ms at $y = 3$ cm. (Note that there has been no consideration here of the effects of possible anisotropy in the inertial subrange turbulence on the dissipation estimates). These timescales are long in comparison to the particle timescales: for the median particle size, the timescale ratio τ_p/τ_K is about 0.1. Snyder and Lumley suggest, reservedly, that their hollow glass beads that had the smallest (0.145) timescale ratio of all the particles used in their experiments possibly behaved like passive scalars. Thus, the timescale ratios above indicate that the sand grains may have behaved like passive tracers of tur-

bulent fluid motions in the inertial subrange. We emphasize the ''may'': the question of how sand grains behave in turbulence is a topic of continuing research (e.g., Nielsen 1992). It is important to note, however, that the energy level in the acoustic velocity measurements (both the ADV and Dopbeam) match the fluid velocity observations of Hussein et al. (1994). In addition, both acoustic instruments successfully resolve the inertial subrange.

It is also worth considering the scale sizes of the highest-frequency fluctuations in Figs. 10 and 12. In the Dopbeam spectra, the highest wavenumber before the noise floor is reached is a little more than 10^2 m^{-1}, corresponding to a particle-laden eddy scale of 3 cm. Thus, the eddies detected by the Dopbeam are large compared to the size of the particles. The Kolmogorov scale for the smallest eddies, on the other hand, is

$$\eta_K = \left(\frac{\nu^3}{\epsilon}\right)^{1/4}. \tag{19}$$

The dissipation rates above give $\eta_K \simeq 1.6 \times 10^{-4}$ cm, corresponding to a wavenumber of about 4×10^4 m^{-1}, well above the highest wavenumbers in Fig. 10.

Finally, recall the broad similarity in the shapes of the hotfilm and Dopbeam spectra (Figs. 10 and 12), at frequencies below the point at which the Dopbeam noise floor is reached. This similarity is consistent with the above timescales: one would not expect the effects of inertial delays in the particle response to appear at frequencies far below $1/\tau_p$.

8. Conclusions

We have presented mean and turbulent particle velocity and concentration measurements made in the laboratory using a coherent Doppler sonar system developed primarily for studies of sediment transport in the oceanic bottom boundary layer. The system has applications to other areas of investigation requiring simultaneous, spatially coincident particle concentration and velocity measurements extending into the inertial subrange of the turbulent kinetic energy spectrum.

The laboratory experiments were carried out using a turbulent jet carrying 180-μm median diameter beach sand. The measurements of mean radial velocity are in good agreement with independent measurements in the present apparatus using a point-sensor laboratory flowmeter (the ADV) and are within 30% of LDV measurements of radial particle velocities presented by Parthasarathy and Faeth (1987). Mean radial velocities computed using entrainment-based models of turbulent round jets are lower than both the Doppler profiler and the ADV measurements by more than 50% near the jet axis. However, agreement between the profiler and the semiempirical theory improves with distance from the jet axis, and the measured entrainment rate ($4.4 \pm 0.6 \times 10^{-3}$ m^2 s^{-1}) is within 10% of the accepted value.

Our computed mean radial velocity profile in the core region of the jet is sensitive to the assumed shape of the axial velocity profile. At least part of the 50% discrepancy is probably due to departures from a true Gaussian shape for W.

Particle radial velocity standard deviations are compared to previous measurements in particle-laden water jets (Parthasarathy and Faeth 1987), and to fluid radial velocity fluctuations in pure momentum air and water jets (List 1982; Hussein et al. 1994). At the centerline, the present observations appear to be consistent (10% agreement) with the pure momentum jet results, provided account is taken of downstream distance. The measured standard deviations fall off smoothly with distance from the jet centerline, as with pure momentum jets. Our measurements also compare well with the particle velocity standard deviations measured by Parthasarathy and Faeth at the jet centerline.

Turbulent kinetic energy spectral densities computed from the Dopbeam radial velocity measurements compare favorably with both the radial and axial ADV velocity measurements. A difficulty in comparing the ADV and Dopbeam is that they are both acoustic systems and they actually measure the speeds of the suspended sand particles. Hotfilm observations were made to provide actual water velocity measurements. The spectral densities computed from the hotfilm have the same shapes, and in particular, they verify the inertial subrange $-5/3$ region seen in the Dopbeam data. In addition, the hotfilm data show that the inertial subrange continues on beyond the region resolved by the Dopbeam and ADV systems. This agreement implies that the sand grains in our experiments may have behaved essentially like passive tracers of the inertial subrange fluid motions, consistent with the findings of Snyder and Lumley (1971) for hollow glass beads in air. Also noteworthy in this respect is the similarity in the shapes of the Dopbeam and hotfilm spectra at larger wavenumbers: similarity in the inertial subrange is difficult to reconcile with a significant nonpassive particle response at these frequencies.

The mean and turbulent particle fluxes in the jet are estimated from the spatially coincident and simultaneous measures of velocity and concentration produced by the coherent Doppler. The net flux is outward from the jet axis. The turbulent flux is roughly half the mean flux but has the same spatial dependence, peaking in the zone of maximum radial gradients in mean concentration and mean axial velocity (presumably also the zone of maximum turbulence production). The turbulent flux is due mainly to the larger scales, presumed to be particle-laden eddies or similar coherent structures. As the measured mean radial flux agrees with estimates computed from entrainment-based theories, the turbulent radial flux must be balanced by divergence of the turbulent axial flux.

The primary goal of the work reported here was to determine the effectiveness of the coherent Doppler system as a momentum and sediment flux sensor at scales comparable to those expected in the wave bottom boundary layer. While improvements can certainly be made, the results are promising and suggest that this technology should indeed provide new and useful insights into mobile sediment dynamics in shallow ocean environments. At the same time, the experiments with the jet point to areas where the present state of understanding of some fundamental questions is still quite limited: in particular, to questions related to the behavior of natural sediment particles in turbulent shear flows. Thus, together with studies of turbulence and particle flux in combined-flow boundary layers, the potential of coherent Doppler sonar for further investigation of particle dynamics in turbulent flows is indicated.

REFERENCES

Brumley, B., R. Cabrera, K. Deines, and E. Terray, 1990: Performance of a broadband acoustic Doppler current profiler. *Proc. Fourth IEEE Working Conf. on Current Measurement,* New York, NY, Institute of Electrical and Electronics Engineers, 283–289.

Buchhave, P., W. K. George, and J. L. Lumley, 1979: The measurement of turbulence with the laser-Doppler anemometer. *Annu. Rev. Fluid Mech.,* **11,** 443–503.

Cabrera, R., K. Deines, B. Brumley, and E. Terray, 1987: Development of a practical coherent acoustic Doppler current profiler. *Proc. Fourth IEEE Working Conf. on Current Measurement,* New York, NY, Institute of Electrical and Electronics Engineers, 93–97.

Chung, J. N., and T. R. Troutt, 1988: Simulation of particle dispersion in an axisymmetric jet. *J. Fluid Mech.,* **186,** 199–222.

Christoffersen, J. B., and I. V. Jonsson, 1985: Bed friction and dissipation in a combined current and wave motion. *Ocean Eng.,* **12,** 387–423.

Fischer, H. B., E. J. List, R. C. Koh, J. Imberger, and N. H. Brooks, 1979: *Mixing in Coastal and Inland Waters.* Academic Press, 483 pp.

George, W. K., and J. H. Hussein, 1991: Locally axisymmetric turbulence. *J. Fluid Mech.,* **233,** 1–23.

Goodman, L., 1990: Acoustic scattering from ocean microstructure. *J. Geophys. Res.,* **95** (C7), 11 557–11 573.

Grant, W. D., and O. S. Madsen, 1979: Combined wave current interaction with a rough bottom. *J. Geophys. Res.,* **84** (C4), 1797–1808.

——, and ——, 1986: The continental shelf bottom boundary layer. *Ann. Rev. Fluid Mech.,* **18,** 265–305.

Hardalupas, Y., A. M. K. P. Taylor, and J. H. Whitelaw, 1989: Velocity and particle-flux characteristics of a turbulent particle-laden jet. *Proc. Roy. Soc. London,* **426A,** 31–78.

Hay, A. E., 1991: Sound scattering from a particle-laden, turbulent jet. *J. Acoust. Soc. Amer.,* **90,** 2055–2074.

——, and J. Sheng, 1992: Vertical profiles of suspended sand concentration and size from multifrequency acoustic backscatter. *J. Geophys. Res.,* **97,** 15 661–15 677.

——, and A. J. Bowen, 1993: Spatially correlated depth changes in the nearshore during storms. *J. Geophys. Res.,* **98,** 12 387–12 404.

Hussein, H. J., S. P. Capp, and W. K. George, 1994: Velocity measurements in a high-Reynolds-number, momentum-conserving, axisymmetric, turbulent jet. *J. Fluid Mech.,* **258,** 31–75.

Lhermitte, R., and R. Serafin, 1984: Pulse-to-pulse coherent Doppler sonar signal processing techniques. *J. Atmos. Oceanic Technol.,* **1,** 293–308.

——, and U. Lemmin, 1990: Probing water turbulence by high frequency Doppler sonar. *Geophys. Res. Lett.,* **17** (10), 1549–1552.

List, E. J., 1982: Turbulent jets and plumes. *Annu. Rev. Fluid. Mech.,* **14,** 189–212.

Lundgren, H., 1972: Turbulent currents in the presence of waves. *Proc. 13th Conf. On Coastal Engineering,* Vancouver, BC, Canada, ASCE, 623–634.

Lynch, J. F., and Y. C. Agrawal, 1991: A model-dependent method for inverting vertical profiles of scattering to obtain particle size spectra in boundary layers. *Mar. Geol.,* **99,** 387–401.

McComb, W. D., 1990: *The Physics of Fluid Turbulence.* Oxford University Press, 572 pp.

Newhouse, V. L., P. J. Bendick, and L. W. Varner, 1976: Analysis of transit time effects on Doppler flow measurement. *IEEE Trans. Biomed Eng.,* **BME-23** (5), 381–387.

——, L. W. Varner, and P. J. Bendick, 1977: Geometrical spectrum broadening in ultrasonic Doppler systems. *IEEE Trans. Biomed Eng.,* **BME-24** (5), 478–480.

Nielsen, P., 1992: *Coastal Bottom Boundary Layers and Sediment Transport.* World Scientific, 324 pp.

Papantoniou, D., and E. J. List, 1989: Large-scale structure in the far-field of buoyant jets. *J. Fluid Mech.,* **209,** 151–190.

Parthasarathy, R. N., and G. M. Faeth, 1987: Structure of particle-laden turbulent water jets in still water. *Int. J. Multiphase Flow,* **13** (5), 699–716.

Pinkel, R., 1980: Acoustic Doppler techniques. *Instruments and Methods in Air–Sea Interaction,* F. Dobson, L. Hasse, and R. Davis, Eds., Plenum Press, 171–199.

Popper, J., N. Abuaf, and G. Hestroni, 1974: Velocity measurements in a two-phase turbulent jet. *Int. J. Multiphase Flow,* **1,** 715–726.

Shuen, J.-S., A. S. P. Solomon, Q.-F. Zhang, and G. M. Faeth, 1985: Structure of particle-laden jets: Measurements and predictions. *A. I. A. A. J.,* **23,** 396–404.

Siegal, D. A., and A. J. Plueddemann, 1991: The motion of a solid sphere in an oscillating flow: An evaluation of remotely sensed Doppler velocity estimates in the sea. *J. Atmos. Oceanic. Technol.,* **8,** 296–304.

Sleath, J. F. A., 1984: *Sea Bed Mechanics.* John Wiley and Sons, 335 pp.

Smith, J. D., 1977: Modeling of sediment transport on continental shelves. *The Sea,* E. D. Goldberg, I. N. McCave, J. J. O'Brien, and J. H. Steele, Eds., Vol. 6, Wiley Interscience, 539–577.

Snyder, W. H., and J. L. Lumley, 1971: Some measurements of particle velocity autocorrelation functions in a turbulent flow. *J. Fluid Mech.,* **48,** 41–71.

Tennekes, H., and J. L. Lumley, 1972: *A First Course in Turbulence.* The MIT Press, 300 pp.

Thorne, P. D., C. E. Vincent, P. J. Hardcastle, S. Rehman, and N. Pearson, 1991: Measuring suspended sediment concentrations using acoustic backscattering devices. *Mar. Geol.,* **98,** 7–16.

Trowbridge, J. H., and Y. C. Agrawal, 1995: Glimpses of the wave boundary layer. *J. Geophys. Res.,* **100,** 20 729–20 743.

Zedel, L., R. Cabrera, A. Lohrmann, and A. Hay, 1995: Single beam, high resolution pulse-to-pulse coherent Doppler profiler. *Proceedings of the IEEE Fifth Working Conference on Current Measurement,* S. P. Anderson, G. F. Appell, and A. J. Williams III, Eds., William S. Sullwood Publishing, 199–204.

——, A. E. Hay, R. Cabrera, and A. Lohrmann, 1996: Performance of a single beam, pulse-to-pulse coherent Doppler profiler. *IEEE J. Ocean Eng.,* **21** (3), 290–297.